

DTIC FILE COPY

4

TECHNICAL REPORT BRL-TR-2951

BRL

1938 - Serving the Army for Fifty Years - 1988

EXPLOSIVE CONSOLIDATION OF COMBUSTION SYNTHESIZED CERAMICS: TiC AND TiB₂

A. NILER
L. J. KECSKES
T. KOTTKE
P. H. NETHERWOOD, JR.
R. F. BENCK

DECEMBER 1988

DTIC
ELECTE
DEC 27 1988
S **D**
E

APPROVED FOR PUBLIC RELEASE; DISTRIBUTION UNLIMITED.

U.S. ARMY LABORATORY COMMAND

BALLISTIC RESEARCH LABORATORY
ABERDEEN PROVING GROUND, MARYLAND

AD-A201 688

DESTRUCTION NOTICE

Destroy this report when it is no longer needed. DO NOT return it to the originator.

Additional copies of this report may be obtained from the National Technical Information Service, U.S. Department of Commerce, Springfield, VA 22161.

The findings of this report are not to be construed as an official Department of the Army position, unless so designated by other authorized documents.

The use of trade names or manufacturers' names in this report does not constitute indorsement of any commercial product.

UNCLASSIFIED

SECURITY CLASSIFICATION OF THIS PAGE

REPORT DOCUMENTATION PAGE

Form Approved OMB No. 0704-0188

1a. REPORT SECURITY CLASSIFICATION Unclassified			1b. RESTRICTIVE MARKINGS			
2a. SECURITY CLASSIFICATION AUTHORITY N/A			3. DISTRIBUTION / AVAILABILITY OF REPORT APPROVED FOR PUBLIC RELEASE; DISTRIBUTION UNLIMITED			
2b. DECLASSIFICATION / DOWNGRADING SCHEDULE N/A						
4. PERFORMING ORGANIZATION REPORT NUMBER(S) BRL-TR-2951			5. MONITORING ORGANIZATION REPORT NUMBER(S)			
6a. NAME OF PERFORMING ORGANIZATION USA Ballistic Research Laboratory		6b. OFFICE SYMBOL (if applicable) SLCBR-TB	7a. NAME OF MONITORING ORGANIZATION			
6c. ADDRESS (City, State, and ZIP Code) Aberdeen Proving Ground, Maryland 21005-5066			7b. ADDRESS (City, State, and ZIP Code)			
8a. NAME OF FUNDING / SPONSORING ORGANIZATION USA Ballistic Research Laboratory		8b. OFFICE SYMBOL (if applicable) SLCBR-D	9. PROCUREMENT INSTRUMENT IDENTIFICATION NUMBER			
8c. ADDRESS (City, State, and ZIP Code) Aberdeen Proving Ground, Maryland 21005-5066			10. SOURCE OF FUNDING NUMBERS			
			PROGRAM ELEMENT NO. 61102A	PROJECT NO. 1L161102AH43	TASK NO.	WORK UNIT ACCESSION NO.
11. TITLE (Include Security Classification) Explosive Consolidation of Combustion Synthesized Ceramics: TiC and TiB ₂						
12. PERSONAL AUTHOR(S) A. Niiler, L. J. Keckes, T. Kottke, P. H. Netherwood, Jr., and R. F. Benck						
13a. TYPE OF REPORT BRL-TR		13b. TIME COVERED FROM FY86 TO FY88		14. DATE OF REPORT (Year, Month, Day)	15. PAGE COUNT	
16. SUPPLEMENTARY NOTATION						
17. COSATI CODES			18. SUBJECT TERMS (Continue on reverse if necessary and identify by block number) SHS, Combustion Synthesis, Explosive Compaction, Ceramics. <i>JES</i>			
FIELD	GROUP	SUB-GROUP				
11	02					
20	13		19. ABSTRACT (Continue on reverse if necessary and identify by block number) A process whereby full density, monolithic ceramic materials are fabricated is described. Elemental powders which are to make up the ceramic compound are reacted by a combustion synthesis process called Self-Propagating High-Temperature Synthesis (SHS). When such a reaction takes place in a properly insulated container, a hot, porous ceramic material is produced which is then compacted to high density by a pressure wave produced by a high explosive. This technique has been used to produce high purity TiC and TiB ₂ at greater than 98% of theoretical density. The size of the plates which can be produced by this method is readily scaleable to the 15 cm range or greater in the lateral dimension and the cost of the ceramics so produced is expected to be lower than with current commercial processes.			
20. DISTRIBUTION / AVAILABILITY OF ABSTRACT <input checked="" type="checkbox"/> UNCLASSIFIED/UNLIMITED <input type="checkbox"/> SAME AS RPT <input type="checkbox"/> DTIC USERS			21. ABSTRACT SECURITY CLASSIFICATION UNCLASSIFIED			
22a. NAME OF RESPONSIBLE INDIVIDUAL A. Niiler			22b. TELEPHONE (Include Area Code) 701 278-4884	22c. OFFICE SYMBOL SLCBR-TB-12		

EXPLOSIVE CONSOLIDATION OF COMBUSTION SYNTHESIZED CERAMICS: TiC AND TiB₂

by

A. Niiler, L.J. Kecskes, T. Kottke, P.H. Netherwood, Jr., and R.F. Benck

U.S. Army Ballistic Research Laboratory
Aberdeen Proving Ground, Maryland 21005

ABSTRACT

A process whereby full density, monolithic ceramic materials are fabricated is described. Elemental powders which are to make up the ceramic compound are reacted by a combustion synthesis process called Self-Propagating High-Temperature Synthesis (SHS). When such a reaction takes place in a properly insulated container, a hot, porous ceramic material is produced which is then compacted to high density by a pressure wave produced by a high explosive. This technique has been used to produce high purity TiC and TiB₂ at greater than 98% of theoretical density. The size of the plates which can be produced by this method is readily scaleable to the 15 cm range or greater in the lateral dimension and the cost of the ceramics so produced is expected to be lower than with current commercial processes.

Accession For	
NTIS GRA&I	<input checked="" type="checkbox"/>
DTIC TAB	<input type="checkbox"/>
Unannounced	<input type="checkbox"/>
Justification	
By _____	
Distribution/	
Availability Codes	
Dist	Avail and/or Special
A-1	



ACKNOWLEDGEMENTS

The authors gratefully acknowledge the contribution of Bart Pierce who did much of the fixture preparations and helped with the explosives operations. We thank Ray Hinksman of Materials Technology Laboratory for running the X-ray diffraction spectra and George Hauver of BRL for help with the ballistic testing.

TABLE OF CONTENTS

	Page
ACKNOWLEDGEMENTS.....	iii
LIST OF FIGURES.....	vii
LIST OF TABLES.....	ix
1. INTRODUCTION.....	1
2. EXPERIMENTAL PROCEDURE.....	4
2.1 Green Compact Preparation.....	4
2.2 Reaction Fixture.....	5
2.3 Explosives Fixture.....	7
2.4 Reaction and Compaction Procedures.....	8
3. RESULTS AND DISCUSSION.....	13
3.1 Product Characteristics.....	15
3.1.1 TiB_2	15
3.1.2 TiC	21
3.2 Parameter Study.....	24
3.2.1 TiB_2	24
3.2.2 TiC	29
3.3 Fabrication Cost Analysis.....	32
4. SUMMARY.....	33
LIST OF REFERENCES.....	35
DISTRIBUTION LIST.....	37

LIST OF FIGURES

Figure	Page
1. A schematic diagram of the reaction, shock compaction assembly showing the sample, container and the explosive charge.....	6
2. Two modes of explosive detonation. 2a shows center initiated wave and 2b shows sweeping wave.....	9
3. Schematic of the fixture used to make in-situ temperature measurements of a reacting sample. Thermocouple and Pyrometer locations are shown.....	10
4. Temperature measurement results for two inch diameter TiC and TiB ₂ samples.....	12
5. Summary of the density vs. C/M data for TiB ₂	16
6. Reacted TiB ₂ sample, showing top and bottom views.....	17
7. Polished surfaces of 98+% dense TiB ₂ . 11a shows commercially available hot pressed TiB ₂ and 11b shows TiB ₂ made by SHS/DC.....	19
8. X-ray Diffraction spectrum for a TiB ₂ sample.....	20
9. Summary of the density vs. C/M data for TiC.....	22
10. Reacted TiC sample, showing top and bottom views.....	23
11. Polished surfaces of 98+% dense TiC. 11a shows commercially available hot pressed TiC and 11b shows TiC made by SHS/DC.....	25
12. X-ray Diffraction spectrum for a TiC sample.....	26
13. Effect of powder mixing on the homogeneity of the reacted and compacted sample, TiB ₂ . 13a shows a high density region and 13b shows a low density region of sample R4.....	27
14. Effect of powder mixing on the homogeneity of the reacted and compacted sample, TiC. 14a shows sample N45 and 14b shows N29.....	30
15. Effect of powder type, graphite vs. carbon black, on the product TiC structure. 15a shows sample N50 and 15b shows R13.....	31

LIST OF TABLES

Table	Page
1. Description of Powders.....	4
2. Titanium Diboride Samples.....	13
3. Titanium Carbide Samples.....	14
4. Best Results.....	15
5. Fabrication Costs by SHS; Current Material Costs.....	32
6. Fabrication Costs by SHS; Future Material Costs.....	33

1. INTRODUCTION

High-technology, structural ceramics are becoming utilized in an ever larger range of applications which require light-weight, high-temperature, high-performance materials. These ceramics are typically the borides, carbides, nitrides and oxides of a variety of metals and are fabricated in such a way as to eliminate most, if not all, porosity and impurities from the bulk. The production of these ceramics involves complicated processes which generally use expensive starting materials, are very energy and labor intensive and so result in very high final product costs.

The most commonly used commercial process for fabricating structural ceramics is hot pressing of the ceramic powder into the shape of a disc, rod or plate. Green (unfired) compacts of ceramic powders are placed into a die in a high temperature furnace and pressed with uniaxial pressure under inert gas atmosphere. While the sample is at high temperature, but well below the melting point of the ceramic, sintering (or solid welding) takes place during which the powder particles coalesce into a solid body. The length of time required for the whole body to be sintered may vary from a few to tens of hours. Since temperatures of 1200 C to 1600 C are quite common, these hot pressing operations can be very expensive from the energy use standpoint. In addition, the high temperature presses with atmospheric control represent a very high capital cost which increases in proportion to the volume of the sample to be processed.

Another means by which high-technology ceramics are fabricated is by Hot Isostatic Pressing (HIP). The major difference between HIP and hot pressing is that in HIP, isostatic rather than uniaxial pressure is exerted on the ceramic body during the high temperature cycle. The sample to be fabricated is enclosed in a metal envelope, usually of tantalum or stainless steel, cold pressed to the desired shape, and then heated to temperatures up to 2000 C under the pressure of a working fluid, usually an inert gas, at a pressure in excess of 120 MPa. The advantage of HIPing over hot pressing is that complicated shapes can be produced. In HIPing, as in hot pressing, sintering is the mechanism by which sample consolidation takes place. However, the equipment and green compact preparation are even more complicated thus raising the product cost higher.

High-technology ceramic materials can also be produced by a process called Self-Propagating High-Temperature Synthesis (SHS). This process involves solid combustion synthesis reactions between constituent powders, reactions which are characterized by very high heats of reaction, reaction temperatures of about 3000 C, and reaction front velocities on the order of a few centimeters per second. It is possible to ignite the powder mixtures with a very small amount of energy at which point the heat of reaction that is released sustains further reaction until the whole sample has been synthesized. Fabrication by SHS has a number of distinct advantages over the conventional processes previously discussed. The fact that it is a high temperature process produces a self-purging effect whereby most contaminants are driven from the sample during the reaction. Since all heat except for the small amount needed for ignition is supplied by the exothermic reaction, the process is highly energy efficient and therefore potentially more economical than the conventional processes since no high temperature furnace is needed. Because the product is formed at a temperature usually exceeding 2000 C,

phases and compositions that cannot be formed at the lower temperatures of conventional processing may be feasible.

The SHS process has been successfully used in a number of applications, both in the US and abroad. Possibly the greatest successes to date have been achieved in the Soviet Union where the manufacturing of ceramic powders such as TiC, TiB₂, SiC and B₄N, among others, is now done commercially. In addition, the Soviets are using SHS to produce tool bits¹, dielectric materials, heater elements and high temperature filters. In Japan, as well as the US, the production of materials by the SHS process has not progressed to the commercial stage as of yet, but work has started on some significant applications. In Japan, corrosion resistant coatings inside of steel pipes have been made by centrifugal compaction during SHS reaction². In the US, applications have been limited to the use of SHS as a source of heat in thermal batteries and aerosol dispersal and as a source of the IR signal in TOW missiles. The thermite reactions that are widely used for field welding of steel are probably the most common application of the SHS reaction principle.

However, there have been serious technical problems associated with the fabrication of full density products by this method. The first is the fact that when mixed powders are reacted by SHS, the product generally exhibits as much as 50% porosity, whereas as little as 0.5% porosity in ceramic materials can be detrimental to performance. The second problem is the cracking of the sample during processing. Gases formed from impurities on the powders are driven off at the high reaction temperatures and can form channels in the sample which become crack initiation sites. Cracking is also caused by the thermal shock to the sample as it cools down from the more than 2000 C to ambient in a very short time. If the sample is mechanically loaded in order to increase its density and its temperature at the time of loading is below the ductile-brittle transition temperature, the internal stresses introduced during such loading may initiate cracking. Another problem is related to the bonding of final product grains to each other. The sample performance depends not only on the absence of porosity but also on the integrity of the inter-granular bonds. The long times at high temperatures needed for sintering action to take place (and its concomitant strong intergranular bonding) is not available for the SHS process since sintering temperatures are sustained for only a few minutes. The final problem is the difficulty in predicting the product properties and synthesis process behavior from the initial powder and compact properties, the initial geometry, and ignition parameters.

Several experiments which utilize the SHS principle to achieve high density products of TiC and TiB₂ have been attempted in US laboratories.

Titanium/Boron and Titanium/Carbon powder mixtures have been heated to ignition inside graphite dies under uniaxial pressure inside high temperature furnaces. Densities of about 95% have been achieved for the reacted product.^{3,4} Ti/B and Ti/C powder mixtures placed inside insulated steel dies have been ignited by tungsten filaments or other small energy sources and reacted. After reaction, the porous product has been compacted by uniaxial pressing in a hydraulic press resulting in densities of about 88%.⁵ Ti/C

mixtures, enclosed in insulated tubes have been ignited and continuously compacted in a rolling mill immediately following the passage of the reaction front. Small areas of high density have been achieved by this method.⁶

Explosives technology has been applied to powdered materials resulting in successful consolidation of both cylindrical and plate forms.^{7,8} Factors affecting the consolidation are the pressure attained, load duration, and the material being compacted. Most commonly, a cylindrically converging system has been used to consolidate high melting point ceramic powders. Starting with Al_2O_3 powders at room temperature, these explosively driven cylindrical compactions have produced material with reasonably pore-free local regions.⁹ However, the degree of compaction has varied with radius and has sometimes been further disrupted by thin spiraled regions of micro-cracked material that occur because the compaction is spatially nonuniform.¹⁰

For ceramic powders, the generally observed result is that large, crack-free specimens of hard, high melting point ceramics cannot be prepared by explosive compaction at room temperature. Aluminum nitride is an exception which is readily consolidated because, it is believed, it becomes plastic at high pressure.¹¹ Partially successful explosive consolidation of ceramic powders has been accomplished by preheating the powders before compaction. Both cylindrical and flat plate samples, crack free and of high density have been made in this way.^{8,12}

Explosive consolidation technology has also been used in SHS ceramics processing. An explosively generated shock wave has been used to attempt both ignition and compaction of Ti/B powder mixtures held in strong containment. The results of this experiment have shown complete SHS reaction of the powders but little or no compaction of the product TiB_2 .³

The processing concept described herein utilizes the SHS reaction to form a porous but hot ceramic body which is compacted to high density by an explosively generated pressure wave. Except for ignition of the SHS reaction, no external heat is applied to the system. The sample is held in insulation to keep it from cooling too quickly after reaction. While its temperature is above the ductile-brittle transition temperature, the explosive charge is set off. This concept is applicable to all shapes which can be made into green compacts and also have the geometrical symmetry to which a shock wave can be applied. No limit is foreseen to the length or width of plates that can be processed. The next section will describe the salient experimental features required for this process. The section following will present the results of these experiments and describes some of the characteristics and properties of the materials produced. In addition, the potentials of this processing method will be discussed.

2. EXPERIMENTAL PROCEDURE

2.1 Green Compact Preparation

The first step in the process is the preparation of the powders and the green compact. The powders used in this work are listed in Table 1. It is advisable to use the highest purity materials since any volatile found on the powder will be driven off, rather violently, by the very high temperatures of the reacting sample.¹³ This action of the impurity gases may disrupt the sample sufficiently to introduce sizeable cracking which may not fuse under any conditions available in these experiments. The optimum titanium powder size have been found to be about -325 mesh. Larger sizes did not react very well in some systems and smaller sizes become too dangerous to handle routinely because of their increased reactivity. Both crystalline and

Table 1. Description of Powders

DESIGNATION	SIZE	PURITY*	DESCRIPTION	MANUFACTURER
Ti-1	-325**	99.7	Titanium	Atlantic (1)
C-1	.05um	90.5	Carbon, Monarch 1300 90.5% fixed C content	Cabot (2)
C-2	.05um	98.0	Carbon, Monarch 1100 98% fixed C content	Cabot (2)
C-3	.05um	99.5	Carbon, Sterling R 99.5% fixed C content	Cabot (2)
C-4	2 um	99.9	Graphite	ConAstro (3)
B-1	-325**	99.5	Boron, Crystalline	Atlantic (1)
B-2	5 um	94-96	Boron, Amorphous	Cerac (4)
B-3	5 um	96.5	Boron, Amorphous	ConAstro (3)
B-4	.07um	99	Boron, Amorphous	Callery (5)

* Manufacturers' Specified Purity in %

** -325 mesh is equivalent to particle sizes less than 44um.

(1) Atlantic Equipment Engineers, Bergenfield, NJ.

(2) Cabot Corp., Boston, MA.

(3) Consolidated Astronautics Inc., Long Island City, NY.

(4) Cerac, Inc., Milwaukee, WI.

(5) Callery Chemical Co., Pittsburgh, PA.

amorphous boron powders in the -325 mesh size were used. The carbon powders that were used were either 2 micron graphite or submicron carbon which agglomerated into several-micron size particles.

The component powders were thoroughly mixed in a ball mill and then uniaxially pressed into green compacts. In order to be guaranteed that the final product composition falls in the region of the binary phase diagrams where the TiC and TiB₂ occur, the titanium/carbon powders were mixed in 55/45 at% ratios and the titanium/boron powders in 33/67 at% ratios. The only requirement on the shape of the compact was that it have symmetry about a plane or axis so as to allow compaction in a direction perpendicular to that plane or axis. In our case, flat discs were the simplest shapes that meet these pressure/symmetry conditions. The only requirement on the pressure at which the green compact be prepared was that it be high enough to keep the compact from falling apart during subsequent assembly. Typically, with the titanium, carbon and boron powders used, this minimum pressure was found to be about 35 MPa.

2.2 Reaction Fixture

The green compact was placed in a gypsum/plaster (CaSO₄·2H₂O) block, made of layers of wallboard epoxied together. The center was cored to a diameter slightly larger than that of the compact. A mild steel ring of about 1 mm wall thickness and height equal to the thickness of the gypsum block was placed between the compact and the gypsum. Two types of steel retainer rings were used in these experiments. The first, labeled HR ring in later discussions, is a single ring with a large number of vent holes which collapses under shock loading. The second, labeled SR ring in later discussions, is made of two separate telescoping pieces, holes only in the top section. The collapse produces less distortion of the steel with this ring than with the HR ring. Both the steel ring and the gypsum block had matching vent holes to the outside of the block. A 0.40 mm thick sheet of Grafoil was placed between the steel ring and the compact leaving about a 3.0 mm space between the Grafoil and the compact. Figure 1 shows a diagram of this assembly.

The first requirement on the reaction fixture was that it contain the sample during the SHS reaction. While the sample is reacting, the movement of volatile gases out of the reaction zone tends to break up the sample, sometimes before the reaction is complete. Thus, the container must be strong enough at the high reaction temperatures (> 2000 C) to keep sample pieces from flying away. The 1 mm thickness of mild steel satisfied this requirement. The container also had to allow the escape of high temperature gases. This was accomplished by providing vent holes in the container wall and leaving ample space between the sample and the inside walls of the container to allow for relatively free gas movement. Another requirement was that the thermal conductivity and heat capacity of the container be low enough so that the heat generated by the reacting sample would not be drained away to the container walls and quench the reaction. This requirement was met by making the steel container a thin, annular ring of low heat capacity and backing the ring with a thermally insulating material such as gypsum. The fact that the gypsum was used for the bulk of the containment vessel satisfied another requirement,

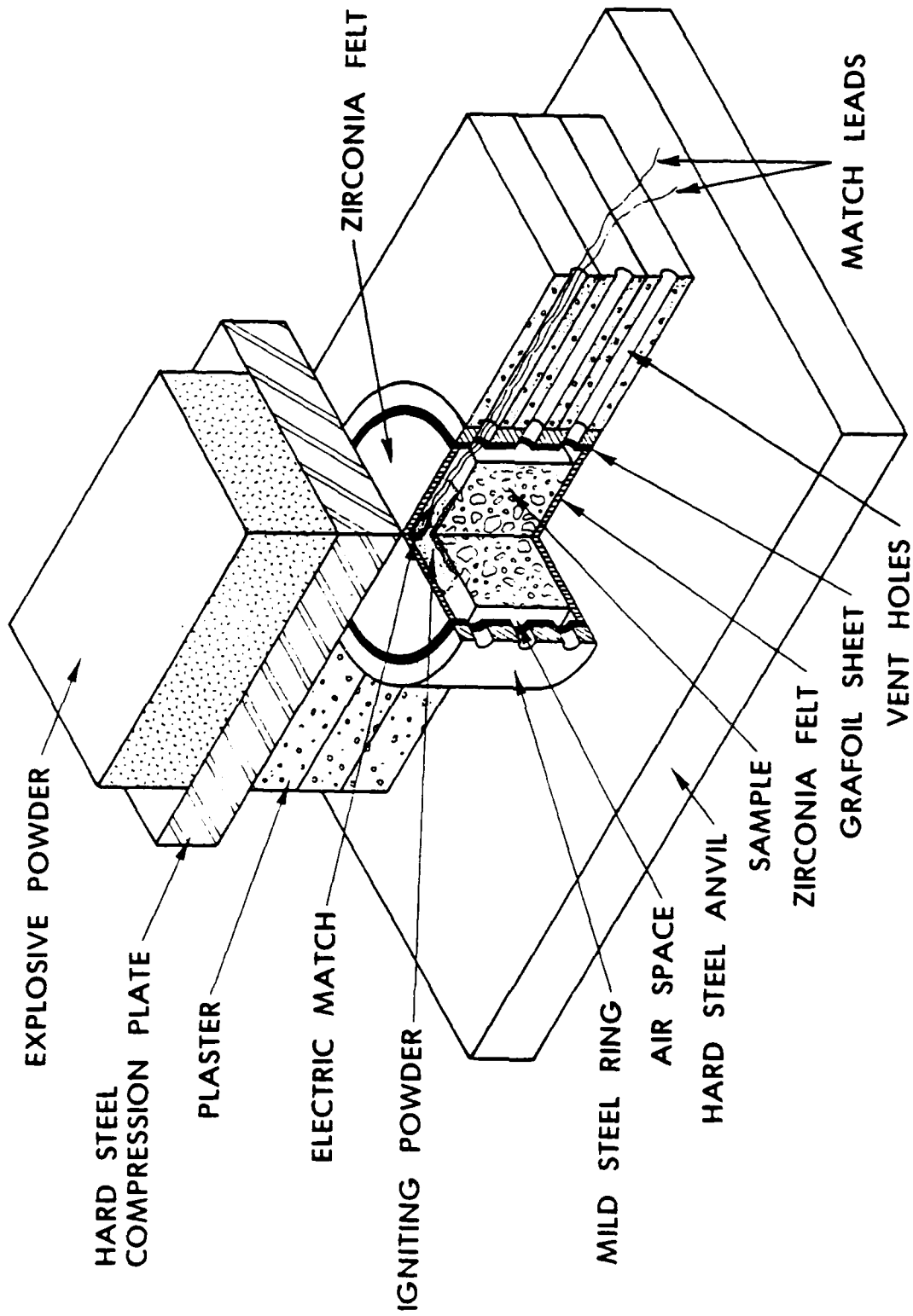


Figure 1. A schematic diagram of the reaction, shock compaction assembly showing the sample, container and the explosive charge.

namely that the compressibility of the container by the explosively generated pressure wave be roughly equivalent to that of the ceramic sample. Finally, Grafoil and Zirconia sheet which are high temperature, relatively inert materials were placed between the sample and the steel container to prevent iron from diffusing into the hot, reacted sample.

The top and the bottom of the containment vessel were made of steel plates with Brinell Hardness Number between 477 and 534, the bottom being the anvil against which the sample was compressed and the top being the compression plate which provided the compaction pressure. Mild steel, rolled homogeneous armor plate (RHA, MIL SPEC 12560), and 4340 steel were also tried but in all cases these softer steels became seriously deformed from the combination of high temperature and shock pressure. Because of this deformation, the samples attained neither full density nor flatness and so the use of all but high hard steel (MIL SPEC 46100) was discontinued. A 1 mm thick sheet of Zirconia insulation was inserted between the steel plates and the compact. A space between the top of the green compact and the insulation was partially filled with the igniter consisting of a mixture of loose titanium (-400 mesh, 4.0 g) and boron (5 micron, 2.0 g) powders with an electric match at the center. The electrical leads from the match were taken out through one of the vent holes to a remote power supply.

2.3 Explosives Fixture

The explosive used in this experiment was Amatol, an 80/20 mixture of TNT and ammonium nitrate. This explosive has been well characterized¹⁴ having a Chapman-Jouguet pressure of 3.75 GPa and a detonation velocity of 3.85 km/sec. This relatively low pressure and detonation velocity makes it suitable for materials which are at a high temperature and thus quite ductile. Using the Mie-Grüneisen equation of state and following the method described by Orava and Wittman¹⁵, the maximum pressure exerted on a hot ceramic sample is 1.65 GPa. However, many of the assumptions and material constants used in this calculation are estimates and the compression plate attenuates the shock considerably. Therefore the actual pressure would be less than the calculated pressure. An experiment to measure the shock pressure was performed using a manganin foil gage placed between the gypsum board and the bottom steel plate in the standard compaction configuration. The pressure recorded at this location was 0.35 GPa. The shock impedances of the gypsum board and the hot ceramic have not been measured so the pressure in the ceramic could not be accurately calculated, but would be higher than the measured pressure. Consequently, the maximum pressure in these experiments was between 0.35 GPa and 1.65 GPa.

The powdered Amatol with a density of 0.86 g/cc was placed in a polymethyl methacrylate (PMMA or Plexiglas) box epoxied on top of the steel compression plate. Two different schemes were used to initiate the detonation. In the first, the detonator was placed at the top center of the box in contact with a small amount of C-3 Detasheet booster in the Amatol powder. With this configuration, a plane shock wave is approximated resulting in close to uniform downward acceleration of the compression plate. In the second scheme, a linewave generator of C-2 Detasheet detonates a length of C-6 Detasheet booster set at one edge of the Amatol powder. With this

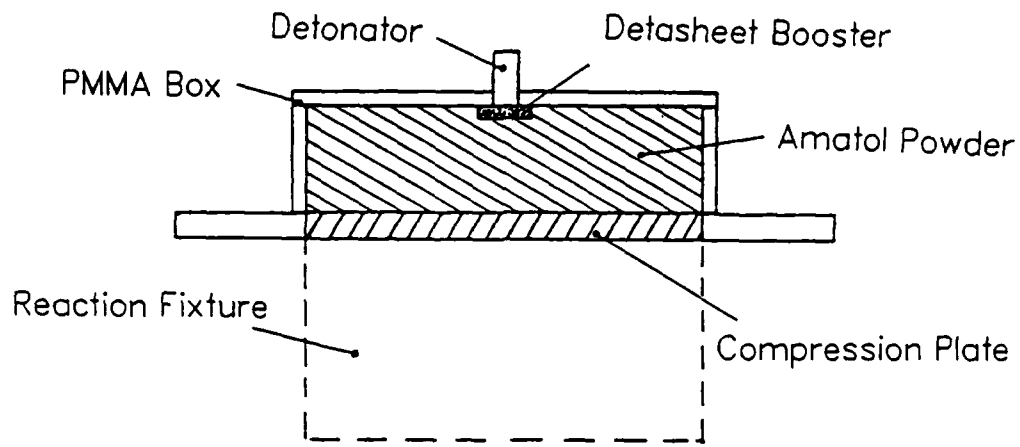
configuration, a sweeping shock wave is generated resulting in grazing incidence compaction. Initiating the explosive in this manner is the condition that allows the compaction of samples of unlimited dimensions lateral to the direction of compaction. The two initiation modes are illustrated in Fig. 2.

2.4 Reaction and Compaction Procedures

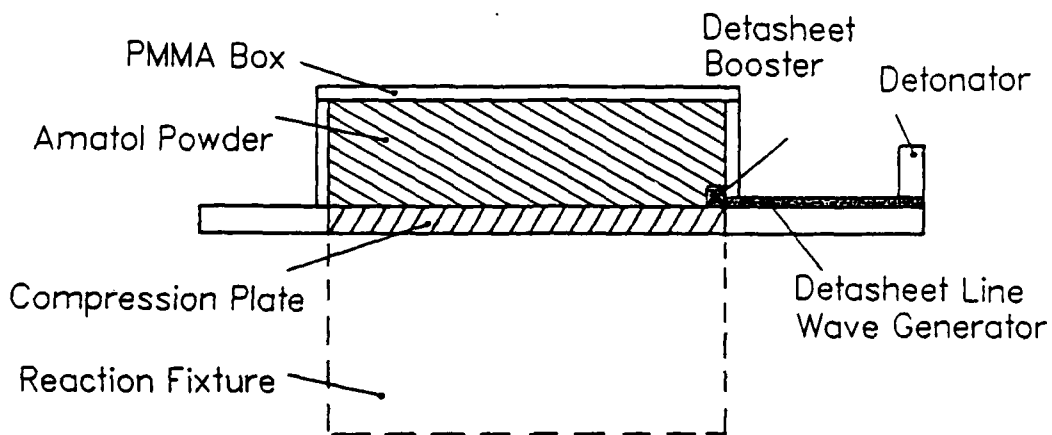
The green compact was ignited by remotely setting off an electric match with a 45 V battery. The burning electric match ignited the loose Ti-B powder at the top of the sample which, in turn, ignited the green compact. The gases released during the combustion escape through the vent holes in the steel ring and backing gypsum container. The heat from the reaction is high enough to not only propagate the reaction through the whole sample, but also to heat the sample to temperatures in excess of 2000 C. Completion of the combustion was verified by either visual observation through a periscope or by thermocouples placed at the bottom of the container vessel. The whole process was also recorded on a Video Cassette Recorder so that the reaction behavior could be analyzed later and any anomalies studied and understood. The reactions generally proceeded to completion within 3 to 10 seconds after ignition.

Once the synthesis reaction was complete, detonation of the explosive was initiated. The effect of the explosion as it propagated over the containment system was to drive the steel compression plate, as a piston, into the hot porous ceramic reaction product and containment fixture. In this manner, consolidation of the ceramic was achieved. It is critical to complete this compression before the temperature of the sample drops below the ductile-brittle transition temperature of the ceramic. As the hot ceramic is compacted by the explosive load, it is further heated by the irreversible work done during compaction. This corresponds to the difference in the pressure-specific volume path during compaction of the porous ceramic from the path in the same space following consolidation as the pressure drops from the compressed state to ambient. This irreversible heating serves to supplement the heating from the SHS reaction and, thereby, to help maintain the thermal conditions necessary for compaction and bonding. The force of the explosion usually buries the newly consolidated and still hot sample under a layer of sand where it is allowed to cool slowly.

An auxiliary experiment was performed to determine the combustion wave speed and the time-temperature history of the reacting samples. These data were needed in order to be assured that the explosive detonation was properly timed; detonation too early would result in incomplete sample reaction and detonation too late would result in the sample having cooled to below its ductile-brittle transition temperature. The schematic of this experimental setup is shown in Fig. 3. Everything was configured as closely to the actual reaction fixture (shown in Fig. 1) as possible and, in fact, interchangeable parts and materials were used. The only differences were that: 1) no explosive was used; 2) Chromel-Alumel thermocouples, whose results are good to about 1200C, were inserted in the sample in the locations shown; and 3) additional holes were machined in the container in order to allow two pyrometers a clear view of the reacting sample surface. One pyrometer measured in the 700 C to 1400 C range and the other in the 1500 C to 3500 C range.



2a. Center Initiation



2b. Sweep Initiation

Figure 2. Two modes of explosive detonation. 2a shows center initiated wave and 2b shows sweeping wave.

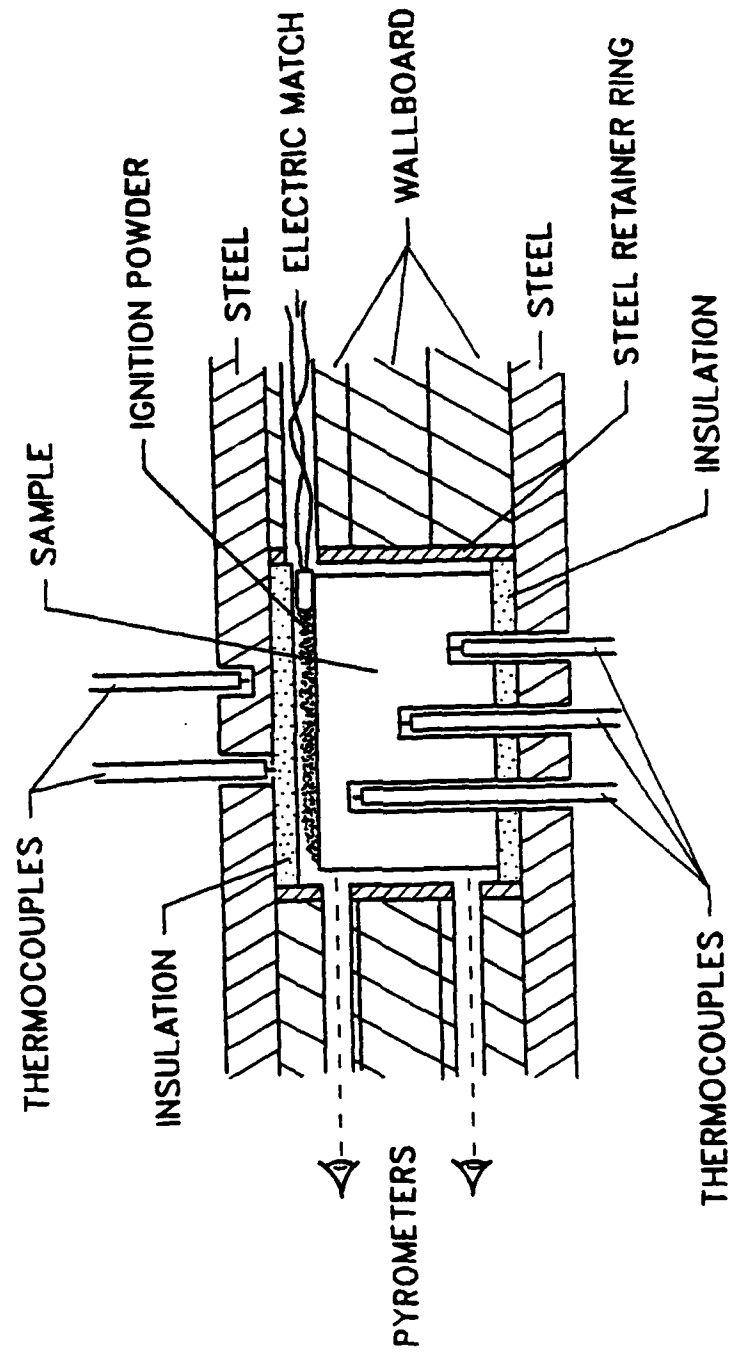
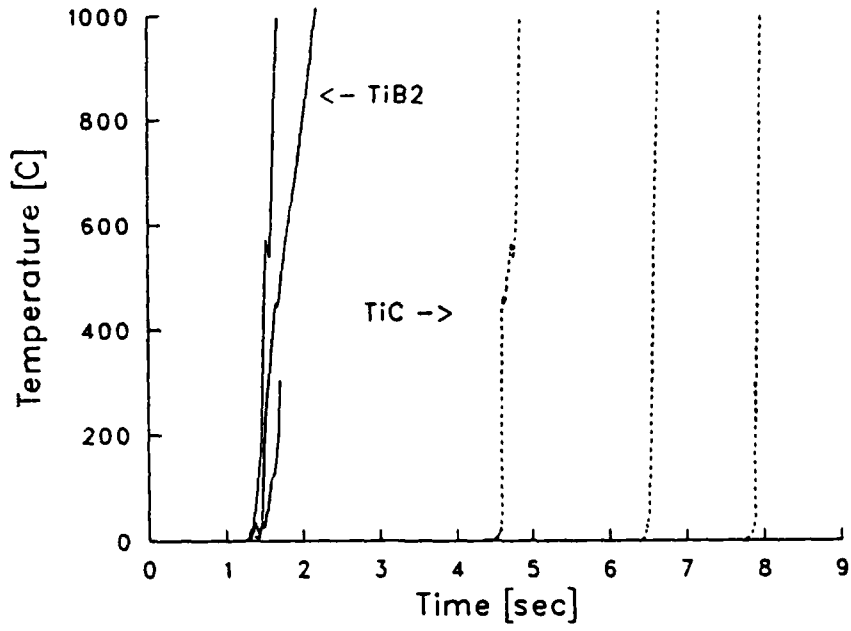


Figure 3. Schematic of the fixture used to make in-situ temperature measurements of a reacting sample. Thermocouple and Pyrometer locations are shown.

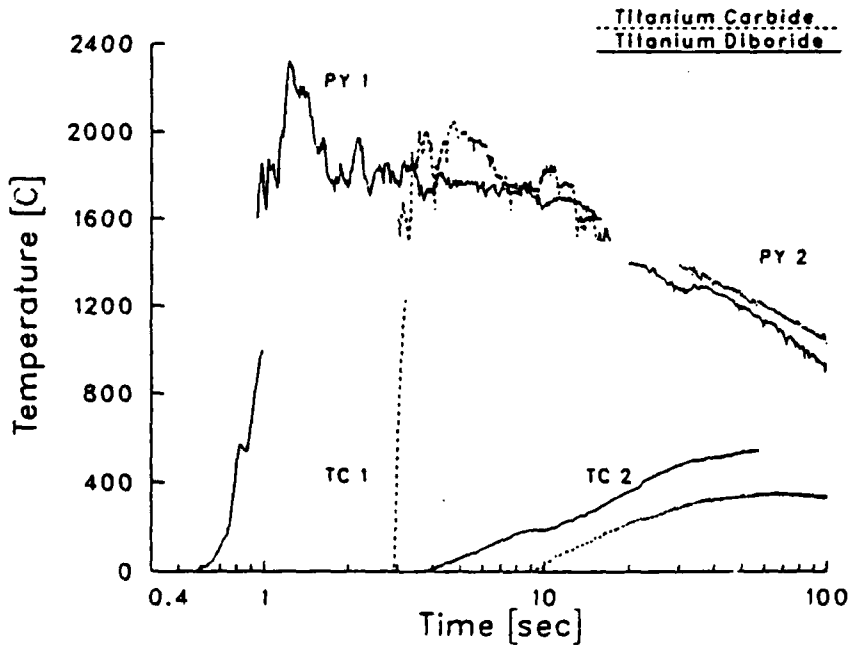
The results of this experiment for TiC and TiB₂ are shown in Fig. 4. Figure 4a shows the temperature-time traces from the three body thermocouples with TiB₂ results on the left and TiC results on the right. Figure 4b shows the temperature-time histories from the two pyrometers and two thermocouples (as labeled) for TiB₂ and TiC. In this figure, the TC 1 refers to the uppermost of the body thermocouples and TC 2 refers to the thermocouple embedded in the top steel plate (see Fig. 3). The results from Fig. 4a show that the TiB₂ reacts much more quickly than the TiC. The fact that all three of the body thermocouples for TiB₂ show the temperature rise at the same time indicates that the combustion wave surrounds the sample and works its way to the interior simultaneously from all sides. On the other hand, the combustion wave for the graphite TiC seems to be well behaved and travels down the sample at a constant velocity. This difference between the TiC and TiB₂ reactions has been observed very consistently and is attributed to the much greater reactivity of the boron as well as the higher heat of reaction for the Ti-B system. The temperature on the surface of the samples, as measured by the pyrometers, is shown in Fig. 4b. The lack of smoothness in these traces is attributed to the pyrometers' views to the samples' surfaces being blocked by flying sample debris and expelled gases. It can be seen that the TiB₂, due to its 50% higher heat of reaction, peaks at a higher temperature than TiC. However, at times greater than 10 sec, the temperatures of the two are about the same, explained by the fact that TiB₂ also has a 50% higher heat capacity.

One of the concerns at the start of these experiments was that the heat of the SHS reaction would raise the top plate temperature high enough to initiate combustion of the Amatom if it were in contact with that plate. This initiation temperature is about 200 C. The results, as shown in Fig. 4b, indicate that the top plate temperature reaches 200 C at about 15 sec for TiB₂ and at about 25 sec for TiC. In light of these results, a thin layer of alumina insulation was always used between the Amatom and the top steel plate so as to allow some flexibility in the timing of the compaction.

Explosive compaction of the hot, reacted TiB₂ was usually initiated at 3 seconds while for TiC, initiation occurred at 10 seconds. Figure 4a shows that these times corresponded to the completion of the reaction. The surface temperatures of both materials are seen to be about 1800 C at these times but core temperatures are expected to be somewhat higher since the surface, not being particularly well insulated, will cool rather quickly at these high temperatures. For a detailed description of this temperature measurement experiment, see reference.¹⁶ Since the ductile-brittle transition temperatures (DBTT) for TiC is in the 800 C to 1200C range,¹⁷ and the DBTT for TiB₂ is in the 1700 C to 2000 C range,¹⁸ this 1800+ C temperature of the samples puts them into the ductile range at compaction time. A possible explanation of why conventional shock compaction experiments typically do not achieve high densities in the final ceramic bodies is the fact that in those experiments the temperatures rarely exceed 1000 C.



4a.



4b.

Figure 4. Temperature measurement results for two inch diameter TiC and TiB₂ samples.

The duration of the pressure pulse on the hot sample is determined by the length of time it takes for the compression plate to come to a complete stop after being set in motion by the explosive. The velocity of a plate in contact with an explosive can be calculated using the Gurney formula.¹⁹ For our experimental situation, this velocity is about 300 m/sec and is the initial, upper limit of the velocity of the compression plate. The plate must move a distance equivalent to the amount that the sample, retainer ring and gypsum wallboard are compacted or 2.5 cm. The lower limit on the time it takes for this compaction to take place is determined by using the initial plate velocity over the 2.5 cm distance, and yields a value of about 85 microseconds. However, the actual compaction time is considerably longer because, during the event, the plate velocity decreases continuously to zero. As a point of reference, conventional shock processing is done with explosives of higher Gurney energy and larger C/M values. These conditions can easily yield a plate velocity close to 3000 m/sec with the consequent factor of ten reduction in the compaction time.

3. RESULTS AND DISCUSSION

Table 2 lists a number of TiB₂ samples fabricated via the SHS/Explosive or Dynamic Compaction (SHS/DC) method showing the variation in the experimental parameters and Table 3 does the same for TiC.

Table 2. Titanium Diboride Samples

Test no	Sample			Explosive			Ring Type	Plate	
	Density (%TD)	Diam (cm)	Boron ID	Thick (cm)	C/M	Init Mode		Area (cm ²)	Thick (cm)
N03	93.9	10.0	B-2	1.9	0.16	SI	HR	413	1.3
N05	80.8	5.0	B-3	1.3	0.11	SI	HR	232	1.3
N06	87.0	5.0	B-3	3.2	0.27	SI	HR	232	1.3
N07	89.7	5.0	B-3	2.5	0.22	SI	HR	232	1.3
N08	87.8	5.0	B-3	1.9	0.16	SI	HR	232	1.3
N09	92.6	5.0	B-3	2.5	0.22	SI	HR	232	1.3
N10	86.9	5.0	B-3	1.9	0.16	SI	SR	232	1.3
N12	89.6	5.0	B-1	1.9	0.16	SI	HR	232	1.3
N14	91.6	5.0	B-3	2.5	0.22	SI	SR	232	1.3
N27	99.7	5.0	B-1	2.5	0.22	SI	SR	232	1.3
N28	94.4	5.0	B-1	3.2	0.27	SI	SR	232	1.3
N32	98.7	15.0	B-1	2.5	0.22	SI	HR	929	1.3
N43	92.9	5.0	B-1	2.5	0.22	SI	HR	232	1.3
N44	94.9	5.0	B-1	3.2	0.27	SI	HR	232	1.3
R04	91.1	5.0	B-1	2.5	0.22	SI	SR	232	1.3
R05	93.0	5.0	B-1	3.8	0.33	SI	SR	232	1.3
R06	92.5	5.0	B-4	2.5	0.22	SI	SR	232	1.3

Table 3. Titanium Carbide Samples

Test no	Sample			Explosive			Ring Type	Plate	
	Density (%TD)	Diam (cm)	Carbon ID	Thick (cm)	C/M	Init Mode		Area (cm ²)	Thick (cm)
N16	90.6	5.0	C-1	3.8	0.22	SI	HR	232	1.9
N19	90.1	5.0	C-1	3.8	0.22	SI	HR	413	1.9
N20	92.5	5.0	C-1	3.8	0.22	CI	HR	232	1.9
N21	89.2	5.0	C-1	1.3	0.07	CI	HR	232	1.9
N22	94.8	5.0	C-1	5.1	0.29	CI	HR	232	1.9
N23	92.0	5.0	C-1	2.5	0.15	CI	HR	232	1.9
N24	95.4	5.0	C-1	6.4	0.36	SI	HR	232	1.9
N25	94.0	5.0	C-1	5.1	0.29	SI	HR	232	1.9
N29	91.4	5.0	C-3	6.4	0.36	CI	HR	232	1.9
N30	90.2	5.0	C-3	5.1	0.29	CI	HR	232	1.9
N37	94.1	5.0	C-1	8.9	0.51	CI	HR	232	1.9
N45	94.2	5.0	C-1	6.4	0.36	CI	HR	232	1.9
N46	96.2	5.0	C-1	7.6	0.44	CI	HR	232	1.9
N47	91.9	5.0	C-2	5.1	0.29	CI	HR	232	1.9
N48	94.3	5.0	C-2	6.4	0.36	CI	HR	232	1.9
N49	88.2	5.0	C-1	3.8	0.22	SI	HR	232	1.9
N50	98.0	5.0	C-1	7.6	0.44	SI	HR	232	1.9
N51	95.0	5.0	C-1	6.4	0.36	SI	SR	232	1.9
N52	93.9	5.0	C-1	7.6	0.44	CI	SR	232	1.9
R01A	96.2	5.0	C-1	7.6	0.44	SI	HR	232	1.9
R01B	97.1	5.0	C-1	7.6	0.44	SI	HR	232	1.9
R01C	96.6	5.0	C-1	7.6	0.44	SI	HR	232	1.9
R02	96.9	5.0	C-1	7.6	0.44	SI	HR	232	1.9
R03	96.6	5.0	C-1	7.6	0.44	SI	HR	232	1.9
R07	93.5	5.0	C-1	7.6	0.44	SI	HR	232	1.9
R12	93.3	5.0	C-4	5.1	0.29	SI	SR	232	1.9
R13	97.5	5.0	C-4	7.6	0.44	SI	SR	232	1.9
R15	94.2	5.0	C-3	5.1	0.29	SI	SR	232	1.9

The notation used in these tables is as follows: the boron and carbon ID codes are from Table 1; C/M is the ratio of the explosive mass to the compression plate mass; center initiation is indicated by CI and sweep initiation by SI; and in the ring type column, HR stands for the retainer rings with a large number of vent holes and SR for the slip ring configuration. In all cases, the plates were made of high hard steel.

The best density and microhardness results for the various sizes of samples that have been made are summarized in Table 4. In this table, commercial hot pressed materials are also included for comparison. Where measured, the results of 1/15 scale ballistic tests in comparison to the hot pressed materials are also shown. These tests²⁰ show that the penetration stopping efficiency of the current best SHS produced TiB₂ is as good as that of the hot pressed. However, the current best SHS TiC showed an efficiency only 70% of hot pressed TiC.

Table 4. Best Results

Material	Dimensions (dia x thk)	Density (% of TD)	C/M	Hardness HK(100g) (kg/mm ²)	Penetration Stopping Efficiency
TiC	5cm x 1.3cm	98+	.44	2000	0.7
TiC	5cm x 2.5cm	90	.22	1400	-
TiC	10cm x 1.3cm	90	.16	1500	-
TiC	15cm x 1.3cm	90	.16	1500	-
TiC	Commercial Hot Pressed	98+		2500	1.0
TiB ₂	5cm x 1.3cm	99+	.22	3200	1.0
TiB ₂	10cm x 1.3cm	92	.16	2000	-
TiB ₂	15cm x 1.3cm	99+	.22	3200	-
TiB ₂	15cm x 2.1cm	98+	.44		-
TiB ₂	Commercial Hot Pressed	98+		3300	1.0

3.1 Product Characteristics

3.1.1 TiB₂. The plot in Fig. 5 summarizes our data on TiB₂, displaying sample densities as a function of the C/M ratio. The open symbols represent samples with amorphous boron while the closed symbols are for crystalline boron. All densities result from measurements of a core taken from the center of the sample, although in most cases, there is very little variation in density from center to edge. Slip ring (SR) data are shown by square symbols and hole ring (HR) data by round symbols. The dashed line is drawn to indicate a general trend of maximum density as a function of the C/M ratio. The data points with numbers fall outside a narrow band around this line; these points will be discussed in a later section. As can be seen, full density TiB₂ is achieved at C/M=0.22, when crystalline boron and a slip ring are used, and when several other conditions which will be discussed later, are satisfied. At higher values of C/M, the samples' densities decrease and they show more fracturing and delamination which are indicative of stronger rarefaction forces and edge effects from the shock wave. The fact that full density of TiB₂ was achieved with the very low C/M value of 0.22 is significantly different from conventional shock compaction work⁸ where the C/M values are routinely in the 5 - 10 range. Other differences between experiments described here and the conventional shock compaction efforts which may play a significant role are the sample temperatures, the duration of the shock pulse, and the morphologies of the powder grains.

Figure 6 shows the top and bottom views of a nearly full density TiB₂ sample, N27. The surfaces are quite smooth, the inner retainer ring has maintained a circular shape through the compaction indicating good containment, and no major cracks are visible on either surface. On lower density samples, views such as these showed considerable cracking and ring distortion and, in some cases, even showed a melting or other failure of the ring. In many of these cases the outer periphery of the sample showed

TITANIUM DIBORIDE Constant M

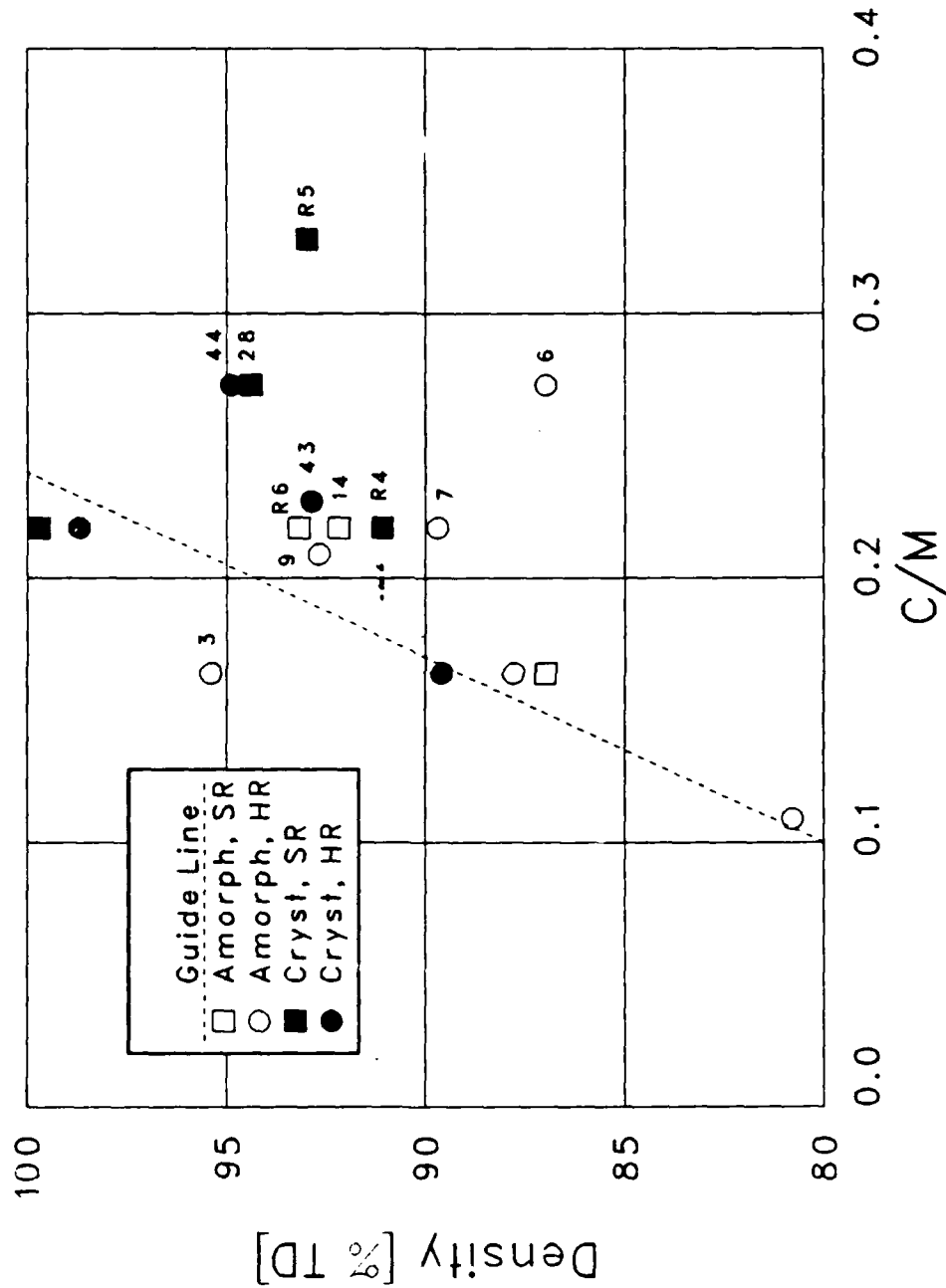


Figure 5. Summary of the density vs. C/M data for TiB₂.

6a. N27 TiB₂ Top View

6b. N27 TiB₂ Bottom View



10 20 30

Figure 6. Reacted TiB₂ sample, showing top and bottom views.

circular cracks, and radial cracks with delaminations appeared throughout the sample. Typically, imperfections such as these occurred at the higher values of C/M. The residue left by the zirconia felt and grafoil can also be seen in this figure. The difference in the surface vs. body temperature described earlier may partially explain the fact that the edges of these samples are usually not as crack-free as the central regions. That is, the lower temperature edges will be less ductile than the center and thus more susceptible to cracking upon compaction. Also, some of the reacting powders can be expelled from the edges by the flow of the hot impurity gases during the reaction. This results in less material at the edges and causes additional edge cracking. Electrical Discharge Machining was used to cut cores from the center parts of this sample in order to determine densities. This very slow and cumbersome procedure was found necessary when the density of TiB_2 samples exceeded about 90% TD because diamond cut-off wheels were no longer effective. In some cases, these cores were used for ballistic testing.

A comparison of the polished surfaces of Hot Pressed and SHS/DC TiB_2 samples is shown in Fig. 7. These SEM micrographs are backscatter electron images and thus have good sensitivity to atomic number differences in various parts of the sample. A variation in the backscatter intensity in the hot pressed sample appears from grain centers to grain boundaries. X-ray analysis showed a slightly larger concentration of tungsten in the grain boundaries than in the grains, a fact sufficient to explain the intensity difference. We have no explanation for the presence of these very small amounts of tungsten. The bright spots scattered about in the grain boundaries contain cobalt and the black spots, all in the grain boundaries, are pores. The shapes of the grains is consistent with expectations when irregularly shaped TiB_2 grains are sintered during hot pressing.

The SHS/DC produced TiB_2 shows a somewhat smaller average grain size than the hot pressed sample. More importantly, however, the shapes of these grains are totally different and are consistent with a section cut through randomly oriented, single crystal grains of hexagonal TiB_2 . One explanation of this single crystal formation is that the reacted TiB_2 melted, probably because of the addition of the shock energy to the reaction heat. The single crystal formation then occurred during cool-down. X-ray analysis of the bright areas in the grain boundaries of the SHS sample show high concentrations of iron. It is significant to note that no iron was observed within the grains. An independent analysis of both the titanium and boron precursor powders by Inductively Coupled Argon Plasma Spectroscopy²¹ shows that both contain about 3 wt% of iron impurity.

An X-ray diffraction spectrum of a typical TiB_2 is shown in Fig. 8 with the peaks attributable to TiB_2 , Fe_2B , and Fe labeled. This spectrum indicates the presence of iron, but the 3 wt% iron shown to exist in the precursor powders cannot be quantitatively verified.

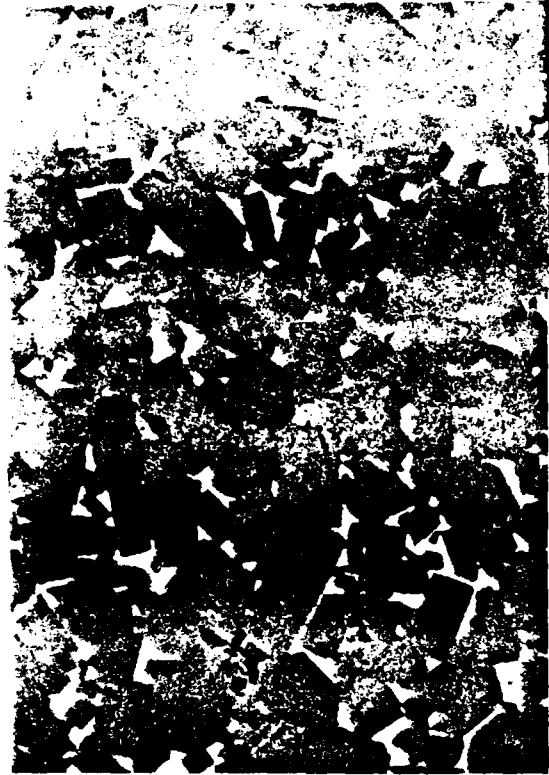
The size distribution of the porosity between the two samples is also different. There is a considerable amount of small sized porosity in the grain boundaries of the hot pressed sample while most of the porosity in the SHS sample is in the form of a few large pores.

7a. Hot Pressed TiB_2



10µm

7b. SHS/DC TiB_2



10µm

Figure 7. Polished surfaces of 98+% dense TiB_2 . 11a shows commercially available hot pressed TiB_2 and 11b shows TiB_2 made by SHS/DC.

TITANIUM DIBORIDE X-Ray Diffraction Spectrum

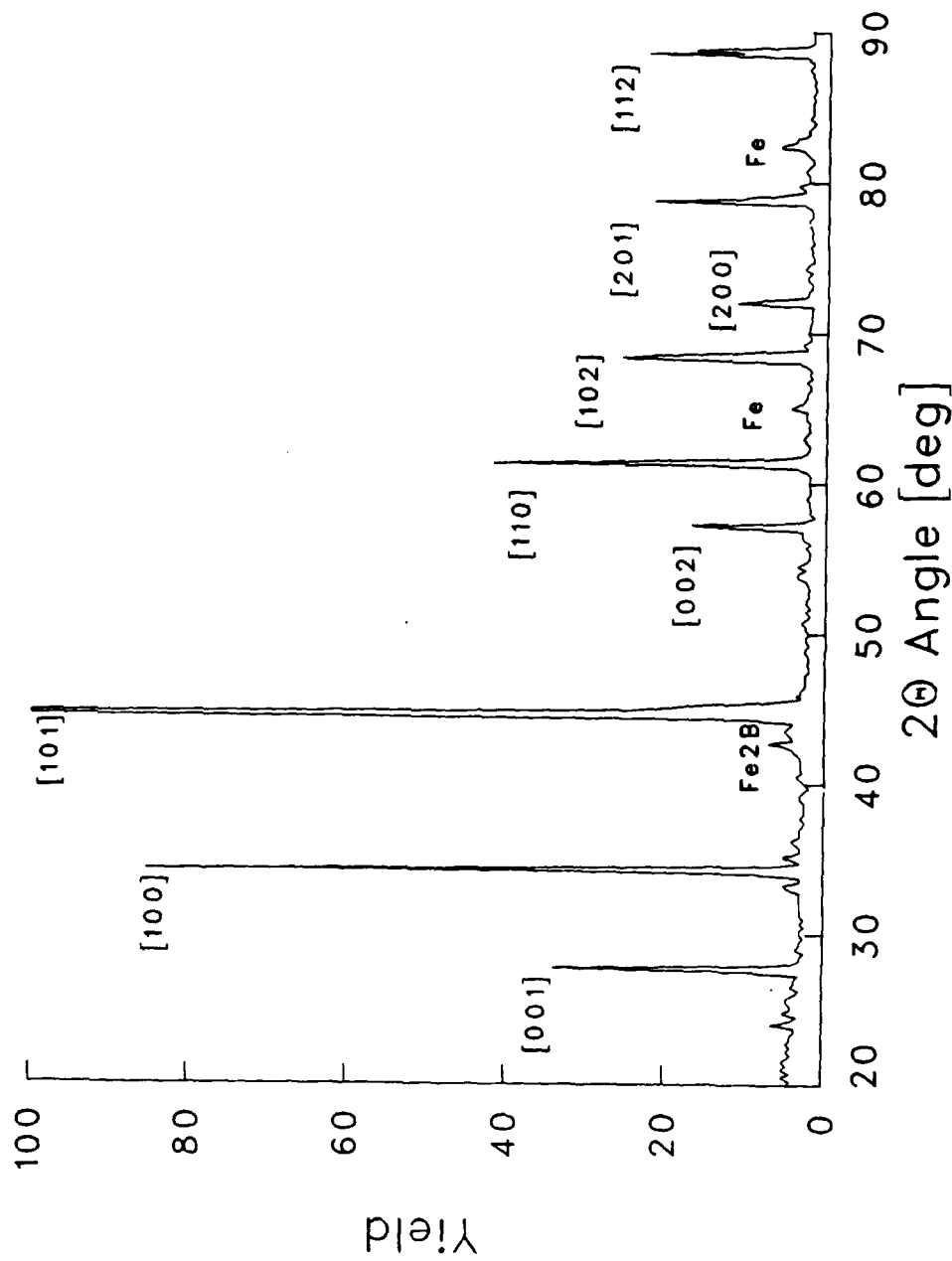


Figure 8. X-ray Diffraction spectrum for a TiB₂ sample.

3.1.2 TiC. The plot in Fig. 9 summarizes the data on TiC. Open symbols represent data with carbon black in the starting compact and the closed symbols represent data with graphite. Experiments with slip rings (SR) are shown with squares and hole ring (HR) data are shown with circles. The dashed line is drawn to indicate a general trend of the maximum density as a function of the C/M ratio. The data points with numbers fall outside a narrow band around this line; these points will be discussed in a later section. In comparing this TiC plot with the equivalent TiB_2 plot (see Fig. 5), it is seen that the highest density results are obtained with C/M values about twice what was needed for TiB_2 . In addition, these highest density results are about 98.5% of TD and not the 99+% observed for TiB_2 . Furthermore, unlike for TiB_2 , the powder type, powder purity, and the type of containment ring used seem not to be significant factors in the density of the TiC.

Additional comparison between the TiB_2 and TiC as listed in Tables 2 and 3 show that a thicker compression plate is used with TiC than with TiB_2 (1.91 cm vs. 1.27 cm). It was found necessary to use the thicker plate to avoid plate distortion and subsequent rounding of the sample faces. The two requirements, higher C/M and thicker compression plate, indicate that the TiC is harder to compact than the TiB_2 . The compressive yield strength of TiC at 1800 C is 50 MPa¹⁷ while that of TiB_2 is 441 MPa.¹⁸ Thus if yield strength, or plasticity, were the only factor involved in compactability, TiC should compact more easily than TiB_2 . Since it does not, another mechanism must be invoked to explain the difference. This other mechanism can be the fact that the temperature of the TiB_2 has exceeded its melting point of 2800 C.²² It is not possible to determine whether this temperature was reached during the reaction or whether the additional energy from the shock was needed. Melting would not occur in TiC because its melting point, 3150 C²², would not be reached even with the additional energy provided by the shock.

Figure 10 shows the top and bottom views of a nearly full density TiC sample, N50. As was the case with the TiB_2 shown in Fig. 6, the surfaces are quite smooth, the retainer ring has maintained its integrity through the compaction, and no major cracks are visible on either surface. On lower density samples, considerable cracking and ring distortion could be observed. On these lower density samples, the outer periphery circular cracks, radial cracks and delaminations appearing throughout some TiB_2 samples were even more accentuated in the TiC. This again indicates a higher resistance to compaction. Additionally, as with the TiB_2 , the temperature gradient from edge to center and the blow-out of material from the edge can be responsible for these 'edge effects'. Cutting cores from the center parts of TiC samples, however, was not nearly as difficult as with TiB_2 and diamond cutoff wheels were very effective even on the highest density samples.

TITANIUM CARBIDE Constant M

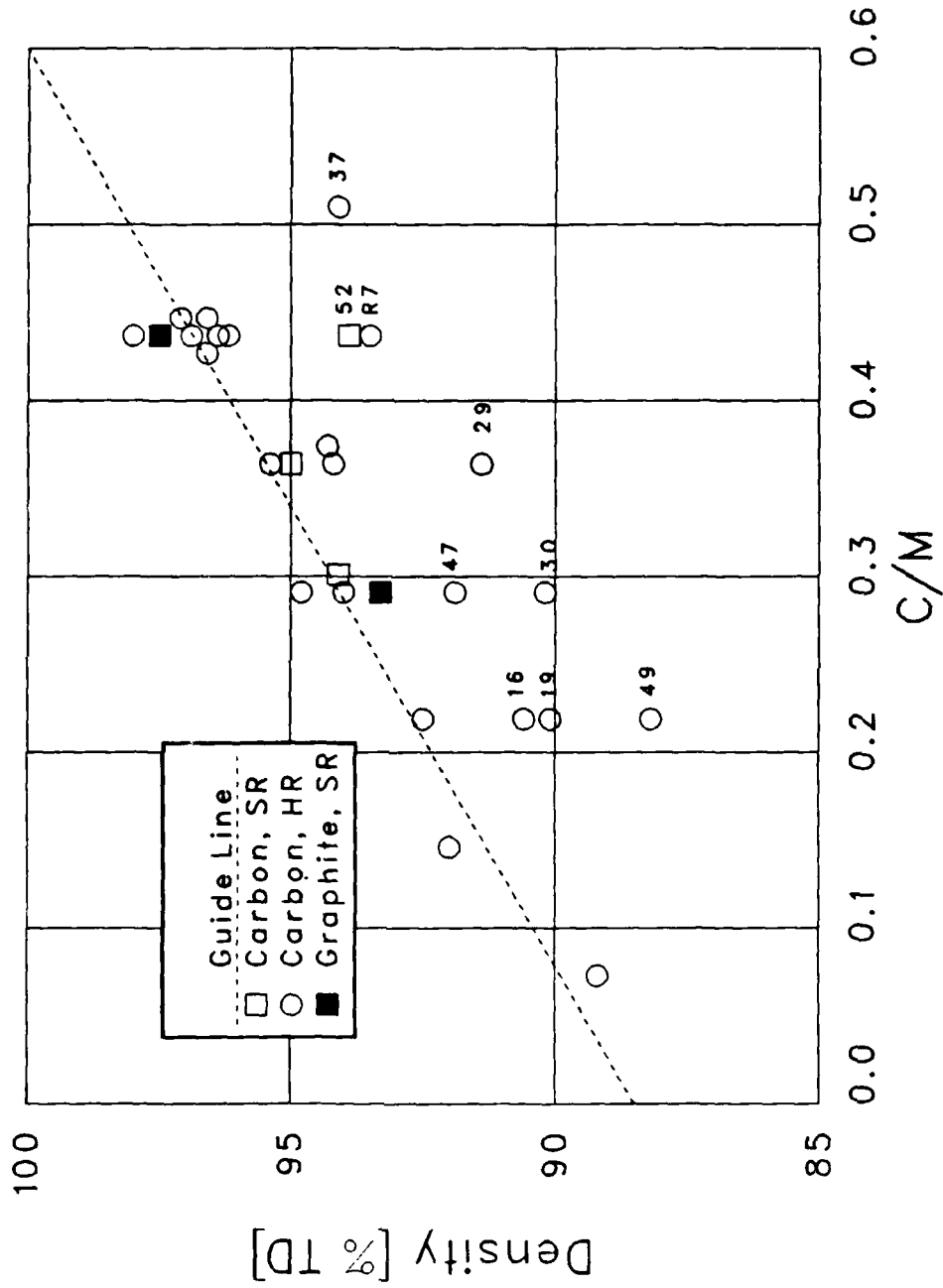
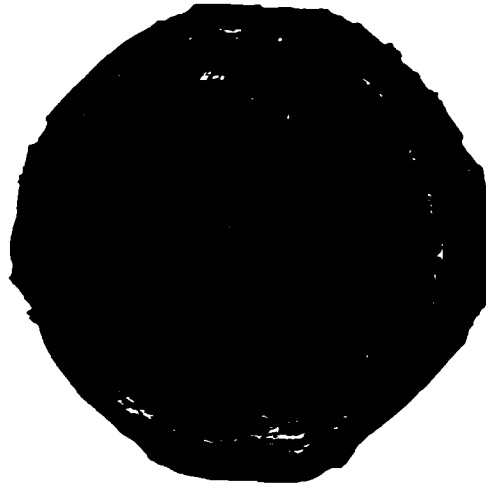


Figure 9. Summary of the density vs. C/M data for TiC.

10a. N50 Tic Top View



10b. N50 Tic Bottom View

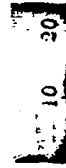


Figure 10. Reacted TiC sample, showing top and bottom views.

Polished surfaces of hot pressed and SHS/DC TiC samples, both with densities of 98% or greater, are shown in Fig. 11. As in Fig. 7, these SEM micrographs are backscatter electron images. Although total porosity is the same in both cases, the pores in the SHS/DC sample are larger than in the hot pressed sample and there are fewer of them. The backscatter intensity from the hot pressed sample is very uniform but the grain size is impossible to determine as no grain boundaries are visible. X-ray analysis did not show any impurities indicating that the TiC powder used as precursor had a very uniform composition and high purity. Although the backscatter intensity from the grains in the SHS sample is very uniform indicating no variation in the titanium to carbon stoichiometry, there is iron in the grain boundaries. The iron originates from the impurity in the titanium powder. Unlike the TiB_2 case, there is no evidence of single crystal formation, indicating that the temperatures probably did not exceed the TiC melting point during the processing.

Figure 12 shows an X-ray diffraction spectrum of a typical TiC sample. The major peak locations and intensities definitively identify the presence of TiC and the absence of any other significant peak indicates the very high purity of the sample. The absence of iron peaks in this spectrum is due to the use of a different, iron-free, titanium powder than was used in the TiC shown in Fig. 11. In all of this work, a Ti/C ratio of 1/.8 was used. As a consequence, all of the TiC peaks are shifted a fraction of a degree from the accepted values given for 1:1 TiC.²³

3.2 Parameter Study

3.2.1 TiB_2 . There seem to be definite effects due to precursor powder type, the quality of preparation, as well as the style of steel retainer ring that was used in both the density and quality of the TiB_2 samples. In Fig. 5, whenever there are data points which should result in the same density but do not, there is an explanation which gives added insight into the processing technique.

At C/M of 0.22, there are two data points showing full density and a number of others in the low 90s. Both of the high density samples were made with crystalline boron, B-1. R4 was made with the same materials and prepared in an identical way to these high density samples with the exception that the powder mixing was done slightly differently. The R4 powders were mixed in a tumbler mixer with mixing rods but no tumbling balls whereas the high density sample powders were ball milled. The effect of this difference in mixing is to leave large agglomerates of boron unbroken resulting in a less intimate contact between the titanium and boron powders. Figure 13 shows polished surfaces of two different areas of sample R4. These micrographs are to be compared with that of sample N27 shown in Fig. 11b.

Figure 13a shows a high density area of R4. Upon comparison with Fig. 11b, two differences are immediately obvious. R4 developed smaller single crystal grains and more pores than N27. The poor mixing left many small unreacted regions some of which probably became nucleation sites for crystal growth while others became pores. Thus the smaller grain size is due

11b. SHS/DC TiC



10 μm

11a. Hot Pressed TiC



10 μm

Figure 11. Polished surfaces of 98+% dense TiC. 11a shows commercially available hot pressed TiC and 11b shows TiC made by SHS/DC.

TITANIUM CARBIDE
X-Ray Diffraction Spectrum

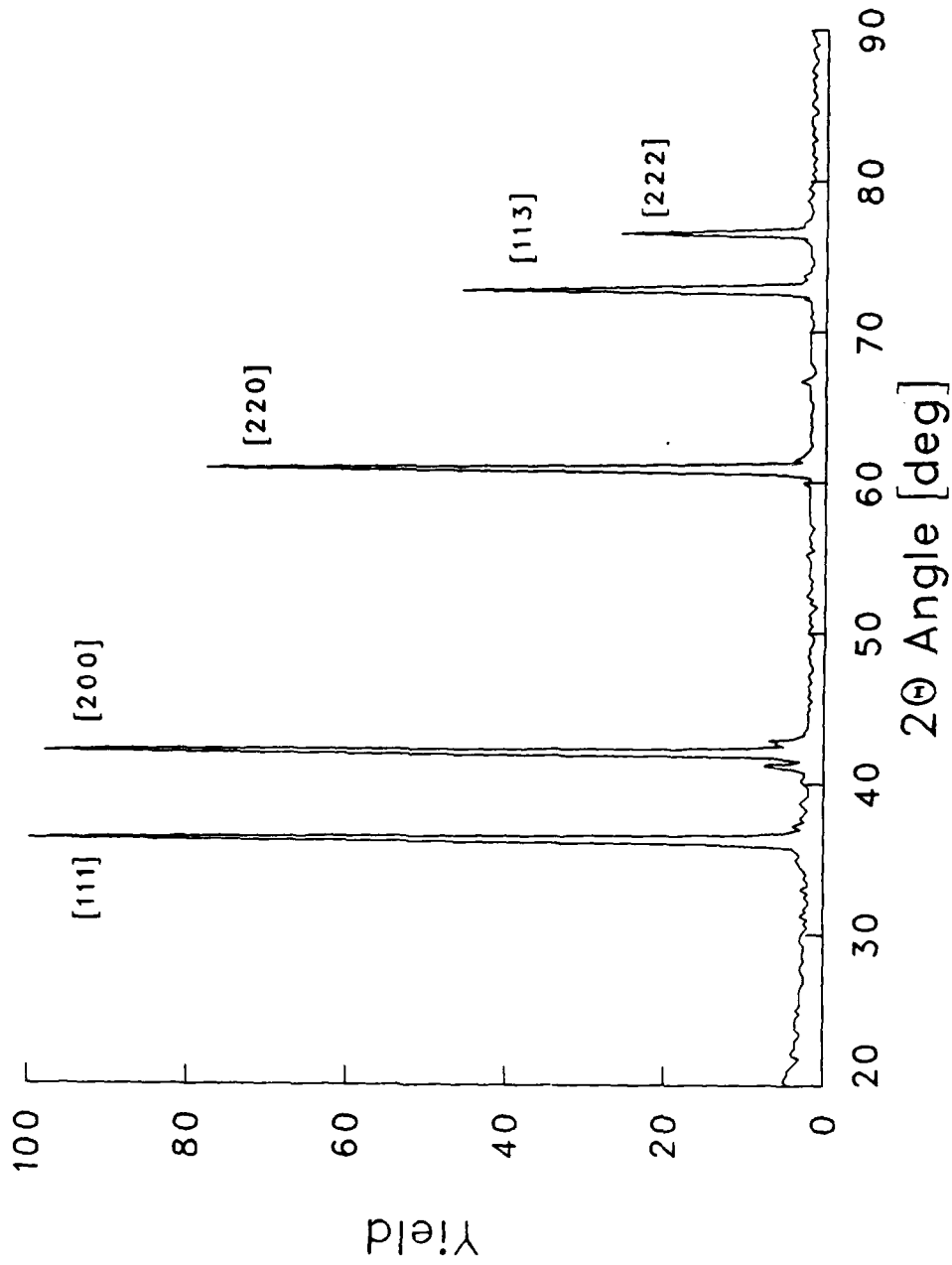


Figure 12. X-ray Diffraction spectrum for a TiC sample.

13a. R4 High Density Area



13b. R4 Low Density Area



Figure 13. Effect of powder mixing on the homogeneity of the reacted and compacted sample, TiB_2 . 13a shows a high density region and 13b shows a low density region of R4.

to the fact that with the larger number of nucleation sites, but same total amount of material, each resulting crystal is smaller. Fig. 13b shows a low density area of R4. The structure seen in Fig. 13b is similar to what is obtained if TiB_2 is fully reacted but not compacted; small regions of full density TiB_2 interlaced with a high degree of continuous porosity. It is speculated that because of the poor mixing and consequent unreacted regions, shock pressure was necessary to both mix and initiate the reaction in these regions. Since the pressure wave was over by the time the shock induced reaction concluded, this region of the sample was left uncompactd.

N43 was also made with the same materials and prepared identically to the high density samples with the exception that an HR ring rather than SR ring was used. The additional force needed to compact the solid HR ring rather than the telescoping SR ring is most likely responsible for the low density of N43. Further evidence that the HR type ring resists compaction at the $C/M=0.22$ level is that whereas N44 at $C/M=0.27$ has a higher density than N43, the reverse is the case for N28 and N27. The conclusion is that at $C/M=0.27$ the lower sample densities are the result of cracking and delamination caused by overdriving with the compacting force rather than resistance by sample or retainer ring.

The samples N7, N9, N14 and R6 were all made with amorphous boron powders and ball milled. Their low densities can be attributed to several possibilities. The first is that because these boron particle sizes were much smaller than the titanium with which they were mixed, there was sufficient mismatch in size to prevent thorough mixing. This would be especially true in the case of R6 which used a very small grained (0.07 micron) boron. The high levels of impurities in these amorphous boron powders, with concomitant gas channel formation during reaction, may also be partly responsible for the resulting lower densities. A third possibility is the small boron particle size which causes a higher combustion rate, thus a more violent expulsion of even small amounts of impurities. The difference between amorphous and crystalline boron shows up at two other C/M ratios, 0.16 and 0.27.

Besides the above three possibilities, sample density can also suffer from retainer ring failure. Such failures can have large effects on specimen quality because they allow the ceramic to spread laterally, reducing the effectiveness of the compaction and causing flow and cracking in the edges of the material. N7 suffered from ring failure, and after several other similar ring failures, it was determined that the rings used in these few experiments were about 1 mm smaller in diameter than called for in the design. This resulted in a smaller air space for gas venting and less space into which the reacting compact could expand. The smaller venting space would result in higher velocity gas flow with larger amount of powder being blown away during the reaction. The smaller expansion volume results in the hot sample making a more intimate contact with the ring thus heating it to a temperature where it can more easily fail.

N43 and the lone HR ring point at full density (N32) present another interesting situation. As can be seen in Table 2, N32 is 15 cm in diameter while N43 is only 5 cm. Since the density data is taken from the central cores, edge effects due to the ring type are less important for the larger sample than for the smaller. Even though the HR ring resists the compaction, the fact that it is further from the center in the larger sample makes its

effect on the core smaller. An alternative hypothesis would be that increasing the size improves heat retention through a reduced surface to volume ratio. N3 was a 10 cm diameter sample and it too shows a density much higher than other data points at the same C/M.

3.2.2 TiC. Whereas powder type, retainer ring type and quality of precursor powder mixing were shown to have significant effects in the densification of TiB_2 , the first two factors do not seem to be important for TiC. Mixing and the manner in which the explosive is initiated do show an effect. Refer to Fig. 9 for the following discussion.

The low densities for samples N29, N30, N47 and R7 can all be attributed to poor mixing. N29 and N30 were made with Sterling R which is a very pure carbon powder and, although the powders were ball milled, they clearly did not mix well. Apparently, when sub-micron carbon particles are very clean, they tend to form very tight agglomerates which are difficult to break up during the ball milling operation. N47 is made with Monarch 1100 which is a much cleaner carbon than Monarch 1300 from which the majority of the TiC samples are made and it too shows poorer mixing behavior and lower final density. Figure 14 shows SEM backscatter electron micrographs of polished N29 and N45 surfaces. N45 is one of the open circle points at C/M=0.37 and density near 94% of Fig. 9. The significant differences between these two samples are the much greater porosity and the large imperfection in N29 which contains unreacted carbon. Clearly, these inhomogeneities which are traceable to poor powder mixing are responsible for not only lower sample density but also act as initiation sites for serious cracking.

The type of carbon powder used, whether graphite or carbon black, did not seem to influence the final density of the product. However, the graphite samples had considerably more horizontal delaminations than the carbon samples. This effect was first noticed when it was discovered that, at C/M values less than 0.3, graphite samples showed very non-uniform thicknesses, much thicker in the middle than at the edges. When the graphite, 99.9% purity, was replaced with Monarch 1300, which was only 90.5% pure, the samples came out quite flat. The difference in the microstructures of TiC made with graphite and carbon black powders is shown in the SEM backscatter electron micrographs of Fig. 15. This figure shows polished surfaces of the two highest density TiC samples, N50 and R13. Although the homogeneity of the microstructure is as good, if not better, in the R13 sample, large inclusions appear throughout the sample. It is speculated that either poor mixing or difficulty in compacting the platelet shaped grains of TiC formed when graphite powders are used is responsible for these inclusions.

N52 is another example of poor results because of a retainer ring whose diameter was too small. See the discussion on TiB_2 sample N7 in the previous section. N37 falls below the line because it may have been overdriven with the resulting cracking and delaminations causing the lower density. Samples N16, N19, and N49 are also seen to be below the line. These three samples, like most of the others at higher C/M values, were compacted with the sweeping wave detonation. The other data at C/M of 0.22, 0.15, and 0.07 were done with center initiated detonation. It is speculated that at these low C/M values where full compaction is not reached anyway, the CI mode, being more efficient and yielding a higher pressure, makes the difference.

14a. N45 Well Mixed

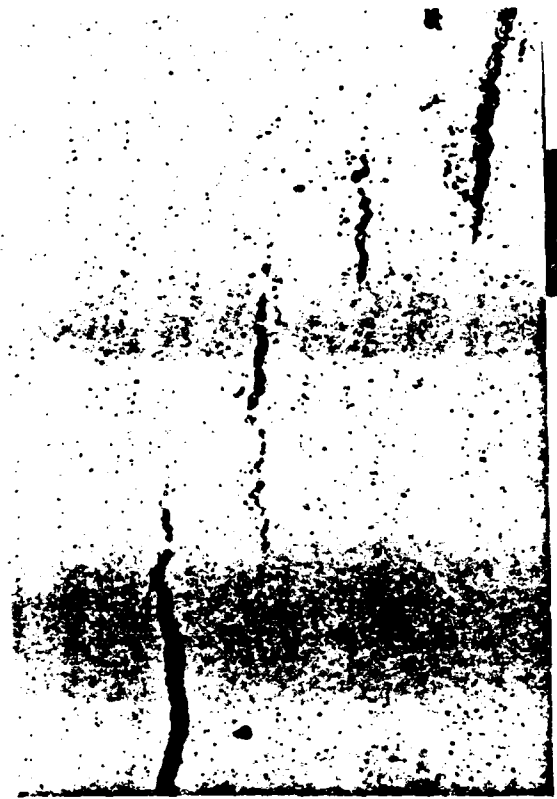


14b. N29 Poorly Mixed



Figure 14. Effect of powder mixing on the homogeneity of the reacted and compacted sample, TiC. 14a shows sample N45 and 14b shows N29.

15b. R13 With Graphite



100µm

15a. N50 With Carbon Black



100µm

Figure 15. Effect of powder type, graphite vs. carbon black, on the product TIC structure. 15a shows sample N50 and 15b shows R13.

3.3 Fabrication Cost Analysis

The high cost of high technology ceramics such as TiC and TiB₂ has been a significant deterrent to their widespread use in large quantity.² The current price of structural TiC and TiB₂ is more than \$90 per kg. This price would have to drop to less than \$25 per kg to be widely used. The following describes an analysis of the costs associated with producing SHS/DC TiC and TiB₂ using the model developed by W. Frankhouser.²⁴ Table 5 shows the summary if current material costs are assumed and Table 6 summarizes the results assuming reductions in material costs based on large quantity purchases and possible new technologies.

In Table 5, the costs of the powders are assumed to be \$ 9.37 per kg for titanium, \$ 220.46 per kg for boron and \$ 2.20 per kg for carbon. In Table 6, reduction in materials cost from a combination of experience curve reductions and some new technologies for producing clean boron powders are assumed so that the costs of the powders are \$ 5.51 per kg for titanium, \$ 33.07 per kg for boron and \$ 2.20 per kg for carbon. Other assumptions in this model are that there is a dedicated facility and personnel in the context of a larger corporation, large scale processing (150 tons/yr), and that all of the technical problems discussed previously in this report are solved with no surprisingly costly solutions. As can be seen, the SHS/DC technique may well lower the cost of TiC and TiB₂ into a range where they can be utilized in large scale. Whether conventional processing can do so also is outside the scope of this report.

Table 5. Fabrication Costs by SHS
Current Material Costs

	<u>TiB₂</u>	<u>%</u>	<u>TiC</u>	<u>%</u>
DIRECT COST (a+b+c)	\$13,241,560	81.3	\$ 3,926,264	73.8
a. Labor (25people)	\$ 768,000	4.7	\$ 768,000	14.4
b. Powders	\$10,754,716	66.0	\$ 1,226,529	23.1
c. Other Materials	\$ 1,718,844	10.6	\$ 1,931,735	36.3
CORPORATION SUPPORT	\$ 318,591	2.0	\$ 132,285	2.5
DIVISION OVERHEAD	\$ 384,000	2.4	\$ 384,000	7.2
CAPITAL DEPRECIATION	\$ 180,000	1.1	\$ 180,000	3.4
G&A	\$ 953,789	5.9	\$ 301,718	5.7
INTEREST	\$ 1,207,835	7.4	\$ 395,541	7.4
TOTAL ANNUAL	\$16,285,775	100.0	\$ 5,319,808	100.0
COST PER KG	\$114.66		\$34.41	

Table 6. Fabrication Costs by SHS
Future Material Costs

	<u>TiB₂</u>	<u>%</u>	<u>TiC</u>	<u>%</u>
DIRECT COST (a+b+c)	\$ 3,245,731	71.9	\$ 2,098,235	66.2
a. Labor	\$ 768,000	17.0	\$ 768,000	24.2
b. Powders	\$ 2,013,107	44.6	\$ 749,577	23.7
c. Other Materials	\$ 464,624	10.3	\$ 580,658	18.3
CORPORATION SUPPORT	\$ 118,675	2.6	\$ 95,725	3.0
DIVISION OVERHEAD	\$ 384,000	8.5	\$ 384,000	12.1
CAPITAL DEPRECIATION	\$ 180,000	4.0	\$ 180,000	5.7
G&A	\$ 254,081	5.6	\$ 173,756	5.5
INTEREST	\$ 336,199	7.4	\$ 236,137	7.5
TOTAL ANNUAL	\$ 4,518,686	100.0	\$ 3,167,853	100.0
COST PER KG	\$ 31.81		\$ 20.50	

4. SUMMARY

A method of fabricating ceramic plates at full theoretical density has been described. Producing the ceramic material itself is accomplished through the combustion synthesis reaction between two or more powdered components. After the highly exothermic synthesis reaction is complete, the ceramic material as formed is highly porous but at a temperature approaching 2000 C. This porous, ductile material is consolidated through the use of a pressure pulse generated by a high explosive acting on a compression plate. This technique has been used to fabricate fully dense (greater than 98% of theoretical density) TiC and TiB₂ in disc shapes 5 cm to 15 cm in diameter and 1.3 cm to 2.1 cm in thickness. The microhardness and ballistic performance values of the SHS TiB₂ equalled those of the hot-pressed materials. However, due to factors relating either to poorer grain bonding or vacancies in the TiC lattice from the sub-stoichiometric ratios of Ti/C, the SHS TiC did not perform as well as the hot-pressed TiC in these two areas. Finally, it was shown that the microstructures of the SHS materials do, in fact, differ from the hot-pressed materials in significant ways leading to the possibility that new and unique structures can be fabricated.

A number of experimental parameters for successful reaction and consolidation have been defined. Due to the very high reaction temperatures in the synthesis step, any volatile impurity will be driven off quite violently causing possibly irreversible damage to the formed material. For this reason, the purest available powders should be used. The reacting sample must be held in containment which is strong enough, must be thermally insulating, must present a low heat capacity to the reacted sample and must be

compressible to the same extent as the sample. The combination of thin-walled steel and gypsum wallboard was found to satisfy these conditions. The volatile gases that are formed must be provided an escape route, a requirement fully satisfied by vent holes in the steel/gypsum container and an air space between the sample and the container. It was determined that high hard steel was best suited as the compression plate, but that TiC and TiB₂ required different thickness plates as well as different amounts of Amatol explosive for best results. For TiC, a 1.9 cm thick plate and 7.6 cm thickness of explosive powder were found necessary. TiB₂, on the other hand, required only 1.3 cm thick plate and 2.5 cm of explosive.

Although only work on the binaries TiC and TiB₂ have been described in this report, this method is applicable to any combustion synthesized material with a high enough heat of reaction to propagate within the necessary containment. Preliminary experiments have been performed with TiC:TiB₂, TiC(Ni), TiB₂(Ni), Al₂O₃:TiC, and HfC²⁵ but a discussion of these materials is outside the scope of this report. In addition, the preliminary economic analysis as described shows that this method has a very high potential of meeting the cost requirements in large scale production.

LIST OF REFERENCES

1. Merzhanov, A.G., Borovinskaya, I.P., Kustova, L.V., and Dubovitskiy, F.I., "Tungsten Free Hard Alloy and Process for Producing Same," U.S. Patent No. 4,431,448, issued 20 February 1980.
2. Odawara, O. and Ikeuchi, J., "Study on Composite Materials with a Centrifugal-Thermite Process," J. Japan Institute of Metals, V.45, No.3, 316-321, 1981.
3. Holt, J.B., "Solid Combustion Processes for Improved Synthesis of Non-Oxide Materials," Lawrence Livermore National Laboratory Report UCRL-94731, June 1986.
4. Zavitsanos, P.D. and Morris, J.R., Jr., "Synthesis of Titanium Diboride by a Self-Propagating Reaction," Ceramic Engineering and Science Proceedings, V.4, No.7-8, 624-633, 1983.
5. Riley, M.A. and Niiler, A., "Low Pressure Compaction of SHS Prepared Ceramics," Ballistic Research Laboratory Report BRL-MR-3574, March 1987.
6. Rice, R.W., McDonough, W.J., Richardson, G.Y., Kunetz, J.M., and Schroeter, T., "Hot Rolling of Ceramics Using Self-Propagating High-Temperature Synthesis," Ceramic Engineering and Science Proceedings, V.7, No.7-8, 737-750, 1986.
7. Stauver, A.M., "Metallurgical Effects Under Shock Compression of Powder Materials," Shock Waves and High-Strain Rate Phenomena in Metals, Ed. Meyers, M.A. and Murr, L.E., Plenum Press, New York, 1981, pp. 865-880.
8. Linse, V.D., "Dynamic Compaction of Metal and Ceramic Powders," Proceedings of the 30th Sagamore Army Materials Research Conference, Lake Luzerne, NY, August 1983, pp. 381-404.
9. Yust, C.S. and Harris, L.A., "Observations of Dislocations and Twins in Explosively Compacted Alumina," Shock Waves and High-Strain Rate Phenomena in Metals, Ed. Meyers, M.A. and Murr, L.E., Plenum Press, New York, 1981, pp. 881-893.
10. Linse, V.D., Adair, J.H., and Shetty, D.K., "Explosive/Dynamic Compaction of Ceramic Powders," UCID-19663-85, V.I, Ed. Cline, C.F., Lawrence Livermore National Laboratory, Livermore, CA, 1985, pp.1-224.
11. Wilkins, M.L., "Dynamic Powder Compaction," UCID-19663-85, V.I, Ed. Cline, C.F., Lawrence Livermore National Laboratory, Livermore, CA, 1985, pp. 329-377.
12. Meyers, M.A., Gupta, B.B., and Murr, L.E., "Shock-Wave Consolidation of Rapidly Solidified Superalloy Powders," Journal of Metals, V.33, 21-25, 1981.
13. Kecskes, L.J. and Niiler, A., "A Study of Impurities in Combustion Synthesis Systems," Ballistic Research Laboratory Report BRL-MR-3658, April 1988.

14. Netherwood, P.H., Jr., "Detonation Velocity Measurements of the Explosives Detasheet C and Amatol," Ballistic Research Laboratory Report BRL-MR-3417, January 1985.
15. Orava, R.N. and Wittman, R.H., "Techniques for the Control and Application of Explosive Shock Waves," in Proceedings of the 5th International Conference on High Energy Rate Fabrication, University of Denver, Denver, CO., 1975, pp. 1.1.1-1.1.27.
16. Kecskes, L.J. and Kottke, T., BRL report to be published.
17. Toth, L.E., Transition Metal Carbides and Nitrides, Academic Press, New York, NY, 1971.
18. Ramberg, J.R. and Williams, W.S., "High Temperature Deformation of Titanium Diboride," Journal of Materials Science, V.22, No. 5, 1815-1826, 1987.
19. Gurney, R.W., "The Initial Velocities of Fragments From Bombs, Shells and Grenades," Ballistic Research Laboratory Report 405, September 1943.
20. Hauver, G.E., BRL Report to be published.
21. Analysis performed by CSTA, Aberdeen Proving Ground, MD.
22. Smithells, C.J., Smithells Metals Reference Book, 6th ed., Butterworth and Company, Ltd., London, 1983.
23. Smith, J.V., Ed., "Powder Diffraction File, Sets 6-10 (revised)," American Society for Testing and Materials, Philadelphia, 1967.
24. Frankhouser, W.L., "Advanced Materials Technology Project; Final Technical Report," System Planning Corporation Report 1121, May 1986.
25. Benck, R.F, Kecskes, L.J., and Netherwood, P.H., Jr., "Preparation of HfC by Dynamic Compaction of Combustion Synthesized Material," Ballistic Research Laboratory Report, to be published.

DISTRIBUTION LIST

No. of Copies	Organization	No. of Copies	Organization
12	Administrator Defense Technical Info Center ATTN: DTIC-DDA Cameron Station Alexandria, VA 22304-6145	1	Commander US Army Aviation Systems Command ATTN: AMSAV-DACL 4300 Goodfellow Blvd St. Louis, MO 63120
1	HQDA (SARD-TR Washington, DC 20310	1	Director US Army Aviation Research and Technology Activity Ames Research Center Moffett Field, CA 94035-1099
1	Commander US Army Materiel Command ATTN: AMCDRA-ST 5001 Eisenhower Avenue Alexandria, VA 22333-0001	1	Commander US Army Communication- Electronics Command ATTN: AMSEL-ED Fort Monmouth, NJ 07703
1	Commander US Army Laboratory Command ATTN: AMSLC-TD Adelphi, MD 20783-1145	1	Commander US Army Missile Command ATTN: AMSMI-RD Redstone Arsenal, AL 35898-5000
1	Commander Armament R&D Center US Army AMCCOM ATTN: SMCAR-MSI Picatinny Arsenal, NJ 07801-5000	1	Commander US Army Missile Command ATTN: AMSMI-AS Redstone Arsenal, AL 35898-5000
1	Commander Armament R&D Center US Army AMCCOM ATTN: SMCAR-TDC Picatinny Arsenal, NJ 07801-5000	1	Commander US Army Tank Automotive Command ATTN: AMSTA-DI Warren, MI 48397
1	Director Benet Weapons Laboratory Armament R&D Center U. S. AMCCOM ATTN: SMCAR-LCB-TL Watervliet, NY 12189	1	Director U.S. Army TRADOC Analysis Center ATTN: ATAA-SL White Sands Missile Range NM 88002
1	Commander US Army Armament, Munition and Chemical Command ATTN: SMCARE-ESP-L Rock Island, IL 61299	1	Commandant US Army Infantry School ATTN: ATSH-CD-CSO-OR Fort Benning, GA 31905-5400

No. of Copies	Organization	No of Copies	Organization
1	Commander US Army Foreign Science and Technical Center ATTN: Mr. Joey F. Crider 220 Seventh Street, NE Charlottesville, VA 22901	4	Director Los Alamos National Laboratory ATTN: Dr. R. Behrens, MST-3C348 Dr. Karl F. Wylie, MS G780 Dr. D. Sandstrom, MS-G756 Dr. S. E. Caldwell P. O. Box 1663 Los Alamos, NM 87545
4	Commander Army Materials Technology Laboratory ATTN: AMXMR-OM Dr. James W. McCauley Dr. Kenneth Gabriel Ms. Theresa M. Resetar ATTN: AMXMR-MCP Dr. Dennis Viechnicki Watertown, MA 02172	1	Director Sandia National Laboratory Applied Mathematics Div 8231 ATTN: Dr. Stephen B. Margolis Livermore, CA 94550
3	Commander US Army Research Office ATTN: Dr. Iqbal Ahmad Dr. Andrew Crowson Dr. Robert Reeber P. O. Box 12211 Res Triangle Park, NC 27709	1	AIRTRON Division ATTN: Dr. John Ings 200 East Hanover Ave. Morris Plains, NJ 07950
1	AFWL/SUL Kirtland AFB, NM 87117	1	ALCOA Laboratory ALCOA Tech Center ATTN: Dr. Aaron J. Becker Alcoa Center, PA 15069
1	Air Force Armament Laboratory ATTN: AFATL/DLODL Eglin AFB, FL 32542-5000	1	General Sciences, Inc. ATTN: Dr. P. D. Zavitsanos P. O. Box 185 Norristown, PA 10401
1	National Bureau of Standards ATTN: D. S. J. Schneider Room A257. Bldg 223 Washington, DC 20234	1	Lockheed Palo Alto Research Laboratory ATTN: Dr. Alexander P. Hardt 3251 Hanover Street Palo Alto, CA 94304
2	Director Lawrence Livermore National Lab ATTN: Dr. J. B. Holt, L-369 Dr. D. Maiden, MS-L71 P. O. Box 808 Livermore, CA 94550	1	Battelle Columbus Laboratory ATTN: Vonne D. Linse Metalworking Section Columbus, OH 43201
		1	Terra Tek, Inc. ATTN: Raymond A. Cutler 400 Wakara Way Salt Lake City, UT 84108

No. of Copies	Organization	No of Copies	Organization
3	Martin Marietta Laboratories ATTN: Dr. Dennis C. Nagle Dr. Stephen R. Winzer 1450 South Rolling Road Baltimore, MD 21227	1	Rice University ATTN: Dr. John Margrave P. O. Box 2692 Houston, TX 77252
3	New Mexico Tech ATTN: Dr. Marc A. Meyers Dr. Naresh Thadani Dr. P. -A. Persson CETR Socorro, NM 87801	1	State University of New York ATTN: Dr. Vladimir Hlavacek Amherst Campus Furnas Hall 507 Buffalo, NY 14260
1	California Institute of Technology ATTN: Dr. T. D. Vreeland Keck Laboratories, MS138-78 Pasadena, CA 91125		Aberdeen Proving Ground Dir, USAMSSA ATTN: AMXSY-D AMXSY-MP, H. Cohen Cdr, USATECOM ATTN: AMSTE-TO-F Cdr, CRDC, AMCCOM ATTN: SMCCR-RSP-A SMCCR-MU SMCCR-SPS-IL
1	Tokyo Institute of Technology ATTN: Dr. Akira Sawaoka 4259 Nagatsuata Midori Yokohama, JAPAN 227		
1	New Mexico Tech ATTN: Dr. Osman T. Inal Materials/Metallurgical Engr. Socorro, NM 87801		
1	Defense Advance Research Project Agency ATTN: Dr. P. A. Parrish 1400 Wilson Blvd. Arlington, VA 22209		
2	Georgia Institute of Tech ATTN: Ms. Kathryn V. Logan Dr. Jesse D. Walton EES/EMSL Atlanta, GA 30332		
1	University of California ATTN: Dr. Zuhair Munir College of Engineering Davis, CA 95616		

USER EVALUATION SHEET/CHANGE OF ADDRESS

This Laboratory undertakes a continuing effort to improve the quality of the reports it publishes. Your comments/answers to the items/questions below will aid us in our efforts.

1. BRL Report Number _____ Date of Report _____

2. Date Report Received _____

3. Does this report satisfy a need? (Comment on purpose, related project, or other area of interest for which the report will be used.) _____

4. How specifically, is the report being used? (Information source, design data, procedure, source of ideas, etc.) _____

5. Has the information in this report led to any quantitative savings as far as man-hours or dollars saved, operating costs avoided or efficiencies achieved, etc? If so, please elaborate. _____

6. General Comments. What do you think should be changed to improve future reports? (Indicate changes to organization, technical content, format, etc.) _____

CURRENT ADDRESS Name _____
 Organization _____
 Address _____
 City, State, Zip _____

7. If indicating a Change of Address or Address Correction, please provide the New or Correct Address in Block 6 above and the Old or Incorrect address below.

OLD ADDRESS Name _____
 Organization _____
 Address _____
 City, State, Zip _____

(Remove this sheet, fold as indicated, staple or tape closed, and mail.)

FOLD HERE

Director
U.S. Army Ballistic Research Laboratory
ATTN: SLCBR-DD-T
Aberdeen Proving Ground, MD 21005-5066



NO POSTAGE
NECESSARY
IF MAILED
IN THE
UNITED STATES

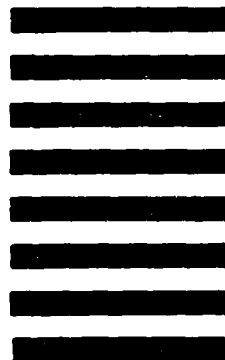
OFFICIAL BUSINESS

PENALTY FOR PRIVATE USE. \$300

BUSINESS REPLY MAIL

FIRST CLASS PERMIT NO 12062 WASHINGTON, DC

POSTAGE WILL BE PAID BY DEPARTMENT OF THE ARMY



Director
U.S. Army Ballistic Research Laboratory
ATTN: SLCBR-DD-T
Aberdeen Proving Ground, MD 21005-9989

FOLD HERE